Research Article Open Access

Witold Żukowski, Przemysław Migas*, Monika Gwadera, Barbara Larwa, Stanisław Kandafer

A numerical analysis of heat transfer in a crosscurrent heat exchanger with controlled and newly designed air flows

https://doi.org/10.1515/chem-2018-0068 received January 16, 2018; accepted May 7, 2018.

Abstract: Simulations of heat transfer between air and flue gases in a plate heat exchanger are presented. The device was designed for the heating of the air supplying a fluidised furnace for the combustion of wet sludge and wood crumbs. The locations of inlets and outlets and the geometry of the heat exchanger are determined by the construction of the furnace. The aim of the simulations was to increase effectiveness of heat transfer through the use of flow redirections with additional baffles placed in the air chamber. The results of the simulations showed that a substantial part of the heat exchanger without baffles is not used effectively. On the basis of a velocity profile, a temperature distribution and a wall heat flux, the geometry of the inter-plate space within the air chamber was modified by adding baffles. The unmodified exchangers had 77% efficiency in comparison to countercurrent exchangers with the same heat transfer area. After the application of baffles, the efficiency increased to 83-91% depending on the construction used (one, two or three baffles). The best model variant of the exchanger with baffles led to the increase in the temperature of air supplying the fluidised bed by approximately 76 K in relation to the system without baffles. Unexpectedly, the presented modifications of the geometry of the system had very low influence of the flow resistance in the air chamber. The value of Δp for the system without baffles is almost the same as for the best model variant.

Keywords: Fluidization; Biomass combustion; sewage sludge; heat transfer modeling; Fluent software.

9

1 Introduction

Combustion in a fluidised bed is frequently used in industrial settings. The fluidised bed furnace ensures a high turbulence in the gas flowing through the crushed solids layer and a good mixing of the latter - this influences the heat exchange rate and, possibly, the mass exchange between the solid and the gas. Such a furnace is characterised by great versatility – it is possible to burn fuels in each state of matter [1]: gaseous [2]-[3], liquid [4]-[5] and solid fuels [6] -[10] in the fluidised bed. Fluidised beds allow the combustion of a number of types of waste, such as polymers[6], rubber fuel [7], [8] or glycerine [5], which are very inconvenient to burn in other types of furnace. It is also possible to burn fuels containing a lot of moisture, such as biomass and especially sludge; however, the combustion of such fuels requires an additional fuel supply, especially at the stage of starting up the furnace – this process can be realised by, for example, cofiring biomass with supporting fuel [11]-[13]. The use of additional fuel is obviously associated with an increase in the cost of thermal disposal. These costs can be minimised through the use of an air heater recuperator, which heats the air supplying the plenum chamber by means of warm exhaust gas - a plate heat exchanger is used for this purpose in the technique presented in the current paper.

Over the past several decades, plate heat exchangers (PHEs) have become essential equipment in a wide range of industries due to their extremely high rates of heat transfer, compactness and flexibility in design and operation. As a result, experimentation and modelling (for example, see refs [14]-[16]) have been used to study the thermal-hydraulic performance of different plate patterns, fouling tendencies, corrosion mechanisms, and fluid flow distributions and to optimize arrangements and configurations. The inter-plate geometry strongly

^{*}Corresponding author: Przemysław Migas, Faculty of Chemical Engineering and Technology, Cracow University of Technology, Kraków, Poland, E-mail: przemyslaw.migas@pk.edu.pl Witold Żukowski, Monika Gwadera, Barbara Larwa: Faculty of Chemical Engineering and Technology, Cracow University of Technology, Kraków, Poland
Stanisław Kandafer: Faculty of Environmental Engineering, Cracow University of Technology, Kraków, Poland

influences the heat transfer efficiency. Experimental research on the use of prototype solutions, however, is very expensive. Computer-aided modelling, using numerical fluid mechanics, can be a useful tool in reducing the costs of testing.

A particularly well-studied procedure is the modelling of heat transfer using a Computational Fluid Dynamics (CFD) tool. Shyam [17] investigated the heat transfer and fluid flow of de-ionized water in a microchannel with parallel plates, both with and without rectangular micromixers (which behave like a roughened surface), as the Reynolds number function. The calculation was made In order to achieve optimised result with maximum heat transfer and minimum pressure drop.

Yaici et al. [18] studied a variety of inlet air flow distributions on in-line and staggered plate-fin and heat exchangers in order to estimate their effects on system performance. The CFD results confirmed the importance of the influence of inlet fluid flow non-uniformity on heat exchanger efficiency. Giurgiu et al. [19] presented a CFD numerical study for two different models of mini channels, to examine the influence of the geometric characteristics on heat transfer intensity, distribution of velocity, temperatures fields and distribution of the convection coefficient along the active mini channel. Pianko-Oprych and Jaworski [20] presented a CFD numerical study for a new design of plate heat exchanger. In this study, two different flow patterns were considered, and it was shown that the geometry of the plates have a strong influence over the fluid flow. CFD analyses can also be applied to a non-Newtonian flow through plate heat exchangers. In work reported in reference [15], single-pass U-type plate heat exchangers with multiple flat plates, with and without baffles, were investigated to analyse this issue.

To summarise, there is great interest in modifying the shape and configuration of plates in order to achieve better heat transfer results. In the present work, the results of simulations of heat transfer in a plate heat exchanger, designed for the heating of air supplying a fluidised bed furnace, are presented. The aim of the CFD simulations was to examine the air velocity in the exchanger plates and to detect 'dead zones' of the flow. In order to eliminate the dead zones in the air flow, the geometry of the interplate space was modified by the application of baffles. Geometries with one, two or three baffles were considered. The benefit of such modifications was the improvement of the exchanger parameters. In particular, inclusion of baffles increases the amount of heat exchanged and results in only a small pressure decrease.

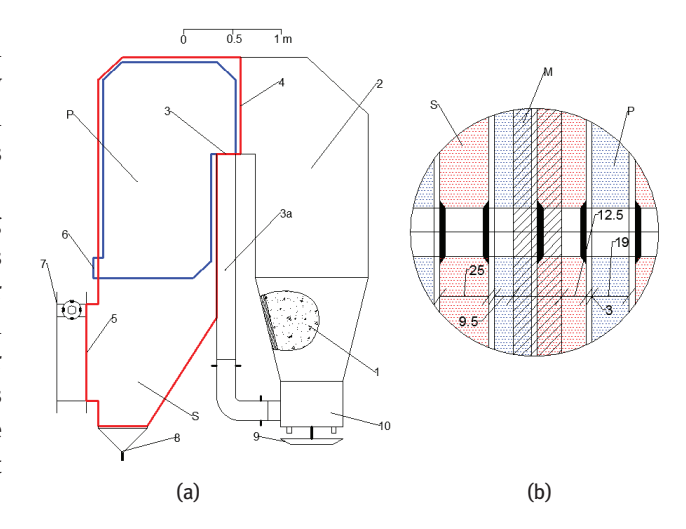


Figure 1: The modelled system: a) The fluidised bed furnace with heat exchanger b) Heat exchanger details: M – control volume (hatched area), S – exhaust gases chamber, P – air chamber, 1 – fluidised bed, 2 – freeboard, 3 – heated air outlet, 3a – pipe supplying heated air to a plenum chamber, 4 – exhaust gases inlet to a heat exchanger, 5 – exhaust gases outlet, 6 – air inlet to a heat exchanger, 7 – water heat exchanger, 8 – ash container, 9 – ash removal system, 10 – plenum chamber.

2 Geometry And Meshing Of Models

The plate heat exchanger was designed to work with the fluidised bed furnace for the combustion of wet sludge and wood chips. This system is schematically presented in Figure 1a. The purpose of installing the exchanger was to heat the air, which was fed into the fluidised bed through a perforated base. The air supplying the reactor flowed through the spaces between the plates of the exchanger, and it was warmed by the hot exhaust gases flowing around the exchanger plates. The system of exchanger plates is shown in Figure 1b.

The first part of the system is a compact structure consisting of a fluidised bed and a freeboard that is dedicated to the combustion of flammable gases carried from the bed; in this section, gases flow from the bottom to the top. The height of this part is determined by the size of the room in which the furnace is located and the residence time of the exhaust gas in the freeboard zone. After leaving the furnace, the exhaust gases pass through a recuperative plate heat exchanger integrated with the freeboard this ensures the compactness of the construction and minimises heat loss; however, it imposes limitations on how the gas is introduced to the heat exchanger and how it exits. As a result of these constraints, the exchanger must be a cross-current exchanger. The bottom part of the exhaust gas chamber ensures pre-dedusting of the gas, which then goes to the exhaust gas-water exchangers. The furnace of the presented structure, with an exchanger that lacks the modifications proposed later in this article, was implemented within the 5th UE framework programme entitled 'FP5 - Energy, Environment and Sustainable Development', project title 'Sludge for Heat' [21]-[22]. The autothermal operation of the furnace was obtained for the combustion of raw sewage sludge with wood chips as an additional fuel.

In order to simulate the heat transfer in the exchanger, a system consisting of two chambers and a steel plate was designed - one chamber was for air and the second was for exhaust gases, and the steel plate separated the two chambers. This layout is presented in Figure 2.

In the actual process, the air flow occurred in 19 chambers, while exhaust gases flowed through 18 chambers. The modelled system of two chambers and a single plate was created in order to minimise the calculation time. The air and exhaust gas chambers were simulated to their symmetry axes. The exhaust gases chamber in the model was 12.5 mm wide, the air chamber was 9.5 mm wide, and the steel plate was 3 mm thick. The heat transfer area on the air side was 2.663 m². The modelled volume is marked in Figure 1b by hatching. In the first step, the air chamber did not have baffles within the gas stream. In the next steps, baffles were added. In order to create a 3D model, Autodesk Inventor was used and then the model was exported to the Design Modeler program from the Ansys 17.2 software package. During the modelling, the heat transfer in the real exchanger (i.e. the system without baffles) was initially simulated, and then one, two and three baffles were added successively (see Figure 3 for a schematic diagram describing selected modifications).

In order to assess the efficiency of heat transfer in all of the configurations tested, the heat exchange in the counter-current heat exchanger with rectangular chambers was also simulated. The heat transfer area (rectangular) was 2.663 m² (approximately 1.2 x 2.21m), which is the same transfer area as in the real exchanger. The widths of the modelled exchanger's parts are the same as for the real system: 9.5 mm, 3 mm and 12.5 mm for the air chamber, steel plate and exhaust gas chamber, respectively. The results of the heat exchange for the real and counter-current systems were then compared. The efficiencies of the studied systems were calculated as the ratio between the average heat flux for the system under consideration and for the counter-current system.

The mesh was made in the grid generator ANSYS Meshing 17.2 and is presented in Figure 2. The multi-zone method of a prism/hexa type was used for the modelling of the air and exhaust gas chambers. For the steel plate, the

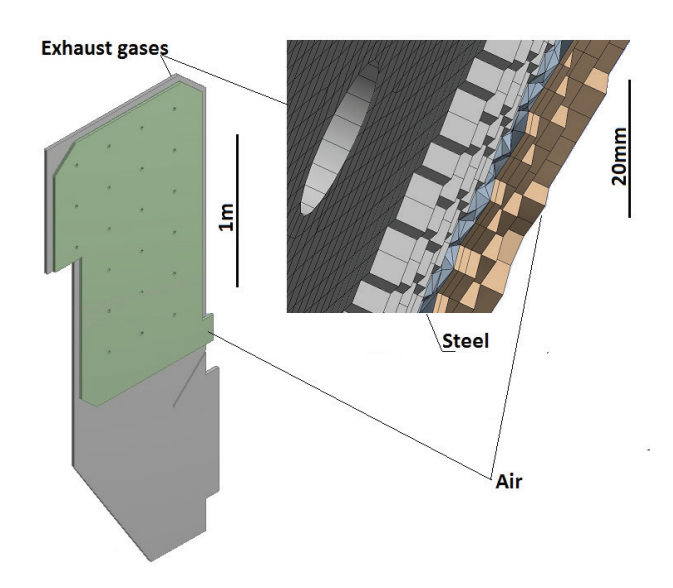


Figure 2: Geometry and mesh of modelled volume.

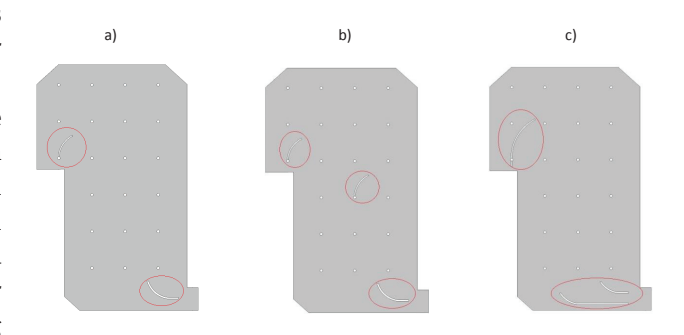


Figure 3: The modified heat exchanger a) two baffles (location of upper and bottom baffles is the same as in the exchanger with one baffle), b) three baffles - version 1, c) three baffles - version 2.

tetrahedrons method with patch conforming algorithm was applied. For the multi-zone mesh, a free mesh was not allowed. The element size for the body sizing was 5 mm. Five divisions were used for the edge sizing. A bias procedure with the bias factor equal to 5 was used. The statistics and quality of the mesh obtained with such settings are given in Table 1. The number of computational elements was 3,025,526 for the real heat exchanger and 2,642,745 for the counter-current heat exchanger. The average orthogonal quality for each exchanger was 0.79845 and 0.81839, respectively, while the average skewness was 0.2783 and 0.25216, respectively. For the cases with baffles, the number of elements ranges from 2,935,586 to 3,607,428, the average orthogonal quality is between 0.79483 and 0.99409 and the average skewness ranges from 0.26157 to 0.2865.

Table 1: Mesh statistics and quality.

Case	Statistics		Quality		
	Number of nodes	Number of elements	Average orthogonal quality	Average skewness	
Counter-current heat exchanger	1,544,738	2,642,745	0.81839	0.25216	
Real heat exchanger	1,945,112	3,025,526	0.79845	0.2783	
Bottom baffle	1,938,635	3,022,645	0.79611	0.28238	
Upper baffle	2,245,782	3,607,428	0.80519	0.26157	
Two baffles	1,889,777	2,935,586	0.79483	0.2865	
Three baffles – ver. 1	1,940,778	3,008,699	0.99409	0.27712	
Three baffles – ver. 2	1,941,978	3,012,853	0.79827	0.27715	

3 Model Set Up And Numerical Approach

In order to simplify the calculations, exhaust gases were represented by an air stream with the same mass flow rate and temperature as in the real process. The inlet temperature was 1173 K for exhaust gases and 300 K for air. The flow was considered to be compressible. The mass flow of air into the modelled volume was 13.45 g/s. The exhaust gas flow was estimated with the assumptions that the air excess factor was 1.5 and that the sludge had a chemical composition close to that of cellulose and contained 50% by mass of water. The resulting stream of exhaust gases (16.80 g/s) was 25% greater than the air stream. The inlet velocity (in the inlet ducts) was 5.81 m/s for air and 4.50 m/s for exhaust gases in the real exchanger and in the exchangers with baffles. For the counter-current heat exchanger, the mass streams of the process gases were the same as for the real exchanger, and the inlet velocities (in the rectangular chambers) were 1 m/s and 3.71 m/s for air and exhaust gases, respectively. The hydraulic diameter in the case of the inlet to the real exchanger and exchangers with wheel ducts was 34.81 mm for air and 48.77 mm for exhaust gases, while in the case of the counter-current exchanger, it was 37.41 mm for air and 48.98 mm for exhaust gases. The turbulence intensity was calculated according to the formula [23]:

$$I = 0.16Re^{-1/8} \tag{1}$$

The calculated intensity was 5%, which is indicative of medium turbulence. A stationary wall with no slip shear condition was set for the wall boundary conditions. Values and relationships of the physical properties of the process

Table 2: Model parameters.

Parameter	Air/Exhaust gases	Stainless steel
Heat cond. coeff. (W m ⁻¹ K ⁻¹)	0.0242	16.27
Heat capacity, (J kg ⁻¹ K ⁻¹)	1006.43	502.48
Density, (kg m ⁻³)	Ideal gas law	8030
Viscosity (Pa·s)	Sutherland law	-

gases and of the steel from which the exchanger's plates were built are presented in Table 2.

The process was considered steady, and the effects of gravity were taken into account. To model heat transfer, the energy equation was enabled in the Ansys Fluent settings. In the modelling, the focus was placed on the heat transport associated with convection in fluid streams and conduction through the wall of the apparatus. The exchange of heat due to radiation was omitted [20][24] by deactivation of the radiation model in Fluent software program.

 The mass conservation equation (or the continuity equation) is

$$\nabla \cdot \left(\vec{\rho v} \right) = 0 \tag{2}$$

2. The momentum conservation equation is

$$\nabla \cdot \left(\rho \overrightarrow{v} \overrightarrow{v} \right) = -\nabla p + \nabla \left(\overline{\overline{\tau}} \right) + \rho \overrightarrow{g}$$
 (3)

where the stress tensor is defined as:

$$\overline{\overline{\tau}} = \mu \left[\left(\nabla \vec{v} + \nabla \vec{v}^T \right) - \frac{2}{3} \nabla \cdot \vec{v} I \right]$$
 (4)

The energy conservation equation is

$$\nabla \cdot (\vec{v}(\rho E)) = \nabla \cdot ((k + k_t) \nabla T) \tag{5}$$

where the total energy is:

$$E = \int_{T_{ref}}^{T} c_{p} dT - \frac{p}{\rho} - \frac{v^{2}}{2}$$
 (6)

The reference temperature was $T_{ref} = 298.15$ K. The turbulent thermal conductivity [25] is:

$$k_{t} = \frac{\overline{c_{p}}\mu_{t}}{Pr.} \tag{7}$$

The turbulent Prandtl number for air and energy Pr. is 0.85. k-ɛ Realisable model was used in the calculation, where k & ε are expressed by the following equations:

The equation for the turbulent kinetic energy k

$$\frac{\partial}{\partial x_i} \left(\rho k \overrightarrow{v_i} \right) = \frac{\partial}{\partial x_i} \left[\left(\mu + \frac{\mu_t}{\sigma_k} \right) \frac{\partial k}{\partial x_i} \right] - \rho \overrightarrow{v_i'} \overrightarrow{v_j} \frac{\partial \overrightarrow{v_j}}{\partial x_i} - g_i \frac{\mu_t}{\rho P r_t} \frac{\partial p}{\partial x_i} - \rho \varepsilon$$
 (8)

The equation for the dissipation rate of turbulent kinetic energy ε

$$\frac{\partial}{\partial x_i} \left(\rho \varepsilon \overrightarrow{v_i} \right) = \frac{\partial}{\partial x_i} \left[\left(\mu + \frac{\mu_i}{\sigma_{\varepsilon}} \right) \frac{\partial \varepsilon}{\partial x_i} \right] + \rho C_1 S \varepsilon - \rho C_2 \frac{\varepsilon^2}{k + \sqrt{\nu \varepsilon}}$$
 (9)

where:

$$C_1 = \max \left[0.43, \frac{\eta}{\eta + 5} \right], \eta = S \frac{k}{\varepsilon}, S = \sqrt{2S_{ij}S_{ij}}$$

The eddy viscosity is calculated from the equation:

$$\mu_t = \rho C_\mu \frac{k^2}{\varepsilon} \tag{10}$$

The realisable k- ε model differs from the standard k- ε and RNG k- ε models in the fact that C_u is not a constant in the realisable model and is instead calculated as a function of the mean strain and rotation rates, the angular velocity of the system rotation, and the turbulence fields (k and ϵ) [23].

The calculations were performed in Ansys Fluent 17.2. The solver type was pressure based. It can be applied for many different flow regimes [23] - incompressible and

compressible, low and high speed. In this type of solver, the velocity field is obtained by solving a pressure or pressure correction equation, which results from the momentum and continuity equations. Two numerical algorithms are available for the pressure-based solver: a segregated and coupled algorithm. In the present work, the segregated algorithm was applied. Therefore, the governing equations were solved separately and sequentially. Since these equations are non-linear and coupled, the solution was iterative - to get a convergent solution, a loop must have been applied.

As the pressure-velocity coupling method, we chose the Semi-Implicit Method for Pressure Linked Equations (SIMPLE) scheme, which is recommended for the steadystate calculations. The system of model equations was solved by the finite difference method with the default setting for the spatial discretization, which included the second-order upwind scheme for the convection terms and the first order upwind scheme for turbulent terms (turbulent kinetic energy and its dissipation rate). The under-relaxation factors for the solution control, used to stabilize the convergence and to prevent the solution from diverging, were set to default settings. The initialization method was hybrid. This type of initialization determines the velocity and pressure fields by solving the Laplace equation; other variables (e.g. temperature, turbulence) are automatically patched. In the applied procedure, the calculations were stopped, when a plateau of the residual curves (the magnitudes of errors for equations in successive iterations) for velocity, continuity, pressure and energy was observed for at least fifty iterations.

Ethical approval: The conducted research is not related to either human or animals use.

Results And Discussion

4.1 Counter-current flow

The counter-current exchanger was simulated as a reference system. The results obtained are presented in Table 3. For the mass flows and inlet velocities applied in the calculations, the air outlet temperature was approximately 869.6 K. The average heat flux was almost 3 kW/m2. The counter-current exchanger had the lowest pressure drop (Δp): 13.7 Pa for air and 10.8 Pa for exhaust gases. This result was, of course, a result of the simple construction of the counter-current exchanger in that the lack of elements caused drastic changes in flow direction and velocity.

4.2 The real system: exchanger without baffles

The results of simulations for the considered systems (and the results for the systems with additional baffles described below) are presented in Figure 4 and in Table 3. The velocity and wall flux charts were performed with the use of user-specified functions with velocities of 0-10 m/s, temperatures 300-1000 K and wall heat fluxes of 0-10,000 W/m². Red indicates areas with values greater than or equal to these extreme numbers, and blue indicates areas equal to the minimum values. The velocity distribution in the analysed exchanger was non-uniform, an issue that negatively influences the effective use of the heat transfer area. The upper and right sections of the air chamber are the areas with the lowest heat transfer, as indicated by the heat flux distribution on the surface of the air chamber wall. These areas were also areas of the highest temperature. The outlet air temperature was 739.5 K. The average heat flux equals 2247.4 W/m². This value constitutes 77.6% of the heat flux transferred in a countercurrent exchanger of the same heat exchange area.

4.3 System with a bottom baffle

The inclusion of a baffle on the bottom of the exchanger was intended to split the main air stream near its inlet and to distribute it to the parts of the exchanger with poorer heat exchange rates, especially the top and the right hand sides. In this configuration, the zone with the highest velocities is located in the central part of the exchanger. The average heat flux was around 2,426.6 W/m², which means an increase of almost 8% in comparison to the system without baffles. This value constitutes 83.8% of the heat flux in the counter-current exchanger. As in the previous case, the area of the highest temperature is located in the top of the air chamber.

4.4 System with an upper baffle

Heat transfer simulations were also conducted for an exchanger that was equipped with an upper baffle. Such a solution enabled the redirection of the stream of air towards the outlet pipe and directing it to the right hand side and top of the air chamber. In this configuration, the heat flux was greater by 9.6% in comparison to the chamber without baffles. As in the previous systems, the considered exchanger is characterised by poor heat transfer in the upper section.

4.5 System with two baffles

The idea behind the inclusion of two baffles (Figure 3a) was to hopefully combine the benefits of the bottom and upper baffles. In reality, a combination of the two effects was obtained. That is, the inlet stream was divided into two streams directed towards the right and top parts of the air chamber, and the stream flowing towards the outlet pipe was returned to the top, right part of the exchanger. In this system, an improvement of the heat transfer conditions in the top part of the exchanger was observed. Its efficiency in respect to the counter-current system was high, reaching 87.5%.

4.6 System with three baffles - version 1

In one solution containing three baffles (Figure 3b), a third baffle was added in the centre of the air chamber of the system containing two baffles in order to distribute the air stream mainly to the right of the exchanger. In practice, this solution turned out to be unfavourable, as the potential gains associated with the redirection of the air stream were reduced by creating a dead zone near the centrally located baffle. The average heat flux was 2465.9 W and the efficiency was 85.2%. These values are lower than for the system with two baffles and similar to the systems with one baffle.

4.7 System with three baffles - version 2

In a second trial with three baffles (Figure 3c), the third baffle was located near the inlet duct, and the upper baffle was made longer. The purpose of such modifications was to improve the inlet air stream dispersion and maximise the effect of redirecting the stream flowing towards the outlet duct in the right and upper directions. There was a significant improvement of heat transfer parameters in this exchanger. In its upper part, the temperature decreased considerably (by at least 1000K). There was a significant improvement of heat transfer parameters in this exchanger. In its upper part, the temperature decreased considerably below 1000K.

The average heat flux was 2655.9 W/m² and was almost 92% of the reference value for the counter-current system. The temperature of the air leaving the exchanger was 815.6 K – this value is significantly greater than for the real heat exchanger and other exchangers with baffles. A similar improvement was found with the heat transfer coefficient

Table 3: Results of modelling.

Case		Counter-current flow	Real system (w/o baffles)	Bottom baffle	Upper baffle	Two baffles	Three baffles – ver. 1	Three baffles -ver. 2
Air	Δ <i>p</i> (Pa)	13.7	147.8	145.5	128.1	131.1	128.01	147.3
	$\mathcal{\delta}_{\scriptscriptstyle C}$ (%)	0.0011	0.003	0.158	0.007	0.0235	0.0461	0.1877
	Heat flux q_{A} , (W m ⁻²)	2895.45	2242.32	2411.40	2457.93	2532.63	2442.98	2467.58
	T_{out} (K)	869.6	739.5	771.7	781.3	795	777	815.6
Exhaust gases	Δ <i>p</i> (Pa)	10.8	20.8	16.9	16.7	22.8	15.6	14.4
	$\delta_{\scriptscriptstyle C}$ (%)	0.00002	0.0408	0.036	0.026	0.067	0.037	0.125
	Heat flux $q_{\rm E}$, (W m ⁻²)	2895.5	2252.5	2441.8	2469.9	2537.2	2488.8	2664.2
Other values	$\delta_{\scriptscriptstyle E}$ (%)	0.0015	0.45	1.24	0.49	0.18	1.84	0.62
	<i>U</i> (W m ⁻² K ⁻¹)	3.325	2.712	2.895	2.977	3.043	2.947	3.209
	Efficiency (%)	-	77.6	83.8	85.1	87.5	85.2	91.7

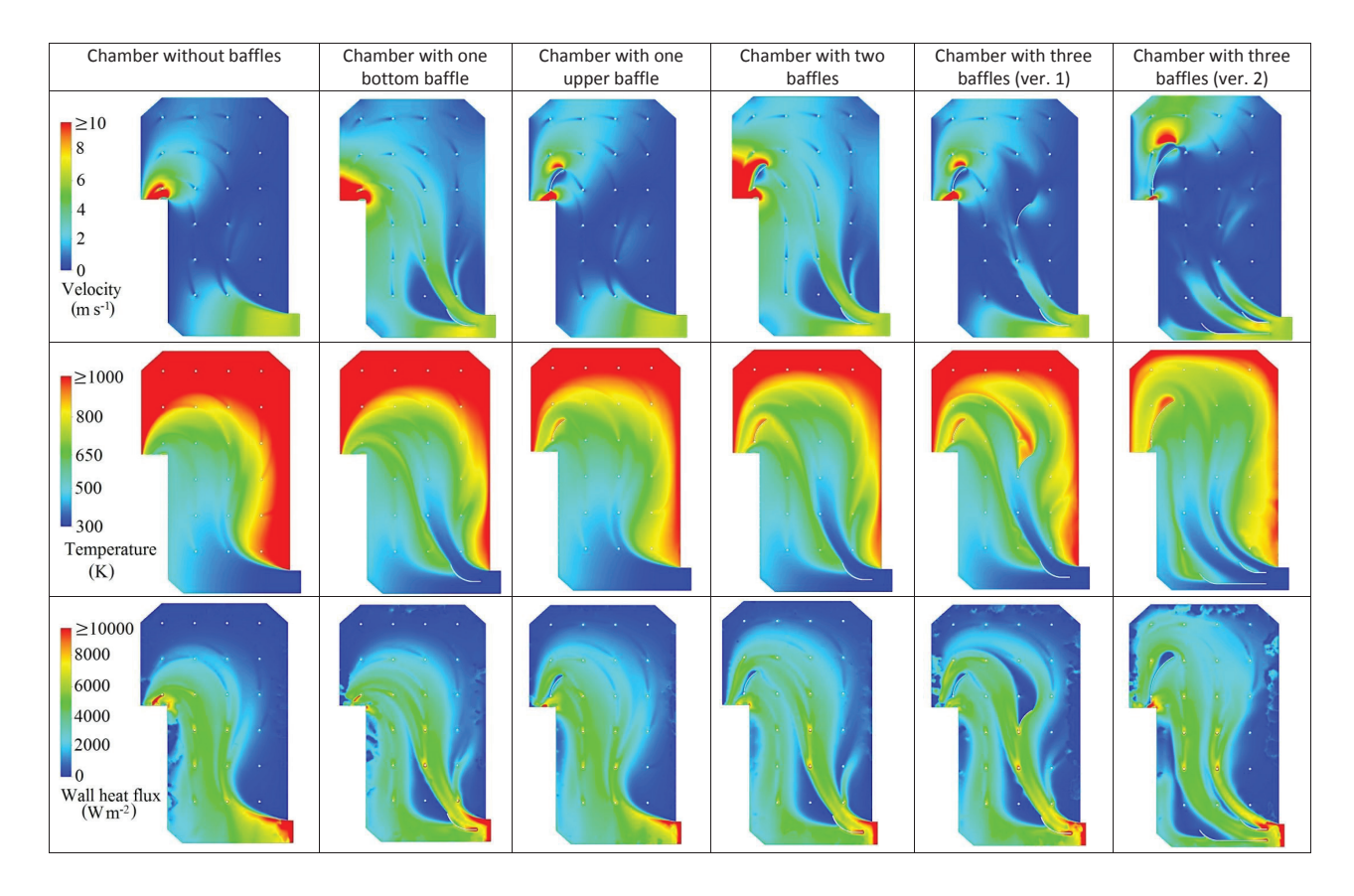


Figure 4: Results of modelling heat transfer in the chambers with different air flow patterns.

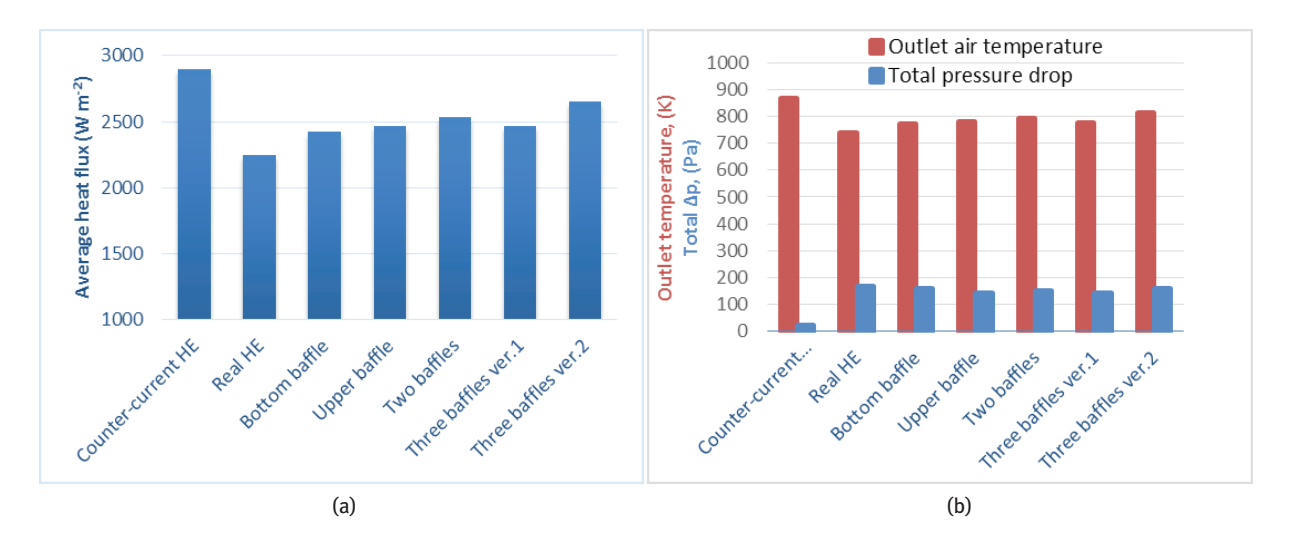


Figure 5: Results of calculations for the considered heat exchanger (HE) geometries: a) Average heat stream, b) Total pressure drop and outlet air temperature.

U: in the second version with three values, the value of *U* is the highest of all the exchangers.

4.8 Summary of results for all considered cases

A comparison of the average heat fluxes for all the considered cases is presented in Figure 5a. The highest value is for the counter-current heat exchanger and the lowest value is for the system without baffles. Of all the exchangers with baffles, the second version with three baffles has the highest average heat flux.

The total pressure drops, defined as the sum of pressure drops for the air and exhaust gases (taken from table 3), are presented in Figure 5b. For the counter-current system, the total drop in pressure is 24.5 Pa. The values for the other cases are greater and range from 140 Pa to 160 Pa. These unexpected $\Delta \mathbf{p}$ results can be explained by the fact that many factors, apart from the baffles, influence the pressure drop, such as the geometry of the entire system (e.g. bends in the exchanger) or the temperature in the inlet ducts (i.e. the fluid velocity at the outlet and the local loss connected with it). When analysing the values of outlet air temperatures presented in Figure 5b, it can be seen that the highest temperature relates to the countercurrent heat exchanger and the lowest temperature relates to the real heat exchanger (the system without baffles). Of all the exchangers with baffles, the highest value is for the second version of the three-baffle exchangers.

Considering the calculation errors presented in Table 3, it can be concluded that the continuity equation errors

are below 0.2%. The situation for the energy balance is slightly worse but remains acceptable, as the calculation errors can reach a maximum of 1.8%; for the best variant, the calculation error is 0.62%.

5 Conclusions

The geometry of a system strongly influences the heat exchange efficiency, which is defined as the average heat flux transferred in a given system in relation to the countercurrent reference system. The modelling results indicate that in the considered exchanger system, the air flows mainly through the central segment, avoiding its upper parts and those located on the right of the exchanger, i.e. above the inlet duct. The efficiency of the system can be increased through the use of baffles, which redirect the air stream in order to eliminate dead zones. In this way, it is possible to achieve a heat exchange efficiency of almost 92% of that achieved with the counter-current heat exchanger and thus to increase the heat flux value by around 18% in relation to the system without baffles.

The conducted modelling indicates that placing baffles in the centre of the system results in an unexpected deterioration in the heat exchange resulting in dead zones near the baffle. A much better solution is to properly modify the space near the inlet and outlet ducts. The main advantage of a baffle near the gas inlet is the division of the centralised air stream into two streams. The use of the baffle near the outlet duct results in a redirection of the air stream towards the right and the top, which improves air flow to the zone characterised by poor heat transfer.

A very important parameter affecting the process of wet sludge combustion is the temperature of the air introduced into the plenum chamber. Proper modifications to the exchanger geometry by means of a baffle system allows the air temperature at the outlet of the recuperator to rise from 740 K for the system without baffles to about 815 K for a system with three baffles (version 2).

The conducted simulations show that the baffle system used has a slight effect on the total pressure drop, the value of which is influenced by both the geometry of the whole system and the temperature in the inlet ducts. In addition, the pressure drop in whole installation is strongly dependent upon flow resistance through fluidised bed (for a bed with a height of 0.5m, this amounts to around 7 kPa). Conflict of interest: Authors state no conflict of interest.

Nomenclature

C_2	adjustable model constant
$\overline{c_p}$	average heat capacity
E g_i	energy the component of the gravitational vector in the <i>i</i> th direction
I	Unit tensor
k	turbulent kinetic energy
k_{t}	turbulent thermal conductivity
m_i	inlet mass flow rate of the gas
• <i>m</i> _o	outlet mass flow rate of the gas
p	pressure
Pr _t	turbulent Prandtl number for energy
$q_{\scriptscriptstyle E}$	heat flux transferred from exhaust
	gases
$q_{_A}$	heat flux taken by air
S	modulus of the mean rate of strain
	tensor
T	temperature
T_{ref} temperature	reference temperature
U	overall heat transfer coefficient
<i>V</i> →	velocity
ν	velocity vector
$\delta_{\scriptscriptstyle C}$	mass balance error
$\delta_{\scriptscriptstyle E}$	energy balance error

ε	turbulent dissipation determines the
	rate of dissipation of the k (turbulent
	kinetic energy)
μ	molecular viscosity
ho	density
$\sigma_{\!\scriptscriptstylearepsilon}$ Prandtl	turbulent Prandtl number for the $\boldsymbol{\epsilon}$
number for the ϵ	dissipation rate
dissipation rate	
σ_{k}	turbulent Prandtl number for the k

stress tensor

References

- Scala F., Fluidized bed technologies for-near zero emission combustion and gasification, Woodhead Publishing, Cornwall,
- Okasha F., Short overview on the jetting-fountain fluidized bed (JFFB) combustor, Renew Sust Energ Rev., 2016, 55, 674-686.
- Okasha F., Smooth combustion of gaseous fuels in a novel configuration of fluidized bed, Fuel, 2013, 106, 512-518.
- Yousefifar A., Sotudeh-Gharebagh, Mostoufi N., Mohtasebi S., Sequential Modeling of Heavy Liquid Fuel Combustion in a Fluidized Bed, Chem. Eng. Technol., 2015, 38, 1853-1864.
- Davidson J.F., Hayhurst, A.N. Menon, A., Scot S., Waller N., Wenting H., The combustion of solid paraffin wax and of liquid glycerol in a fluidised bed, Fuel, 2017, 199, 447-455.
- [6] Burges F., Fennel P.S., Hayhurst A.N., Lloyd P.D.W., Combustion of polymer pellets in bubbling fluidised bed, Combust Flame, 2011, 158, 1638-1645.
- [7] Chyang C., Duan F., Hsu S., Tso J., Combustion behavior and pollutant emissions of batch fluidized bed combustion, J Taiwan Inst Chem Eng, 2013, 44(6), 1034-1038.
- Bautista D. Carmen M. Jul C. Jul R. Mastral A.M. Rodríguez A. Rodríguez M.A., AFBC of coal with tyre rubber Influence of the co-combustion variables on the mineral matter of solid by-products and on Zn lixiviation, Fuel, 2013, 106, 10-20.
- Kijo-Kleczkowska A., Kosowska- Golachowska M., Luckos A., Musiał T., Wolski K., Oxy-combustion of biomass in a circulating fluidized bed, Archives of thermodynamics, 2016, 37, 17-30.
- [10] Baron J., Kandefer S., Kaniowski W., Olek M., Żukowski W., Carbon shale combustion in the fluidized bed reactor, Polish Journal of Chemical Technology, 2014, 16(2), 74-76.
- [11] Awad M., El-Emam S., Okasha F., Zaater G., Zeidan E., Co-combustion of biomass and gaseous fuel in a novel configuration of fluidized bed: Thermal characteristics, Energy Convers. Manage., 2014, 84, 488-496.
- [12] Awad M., El-Emam S., Okasha F., Zaater G., Zeidan E., Co-combustion of biomass and gaseous fuel in a novel configuration of fluidized bed: Combustion characteristics, 2014, Fuel, 133, 143-152.
- [13] Hachicha A.A., Ghenai C., Thermal Performance of Biomass-Fired Steam Power Plant, J. Thermal Sci. Eng. Appl, 2017, DOI: 10.1115/1.4035926.

- [14] Abu-Khader M.M., Plate heat exchangers: recent advances, Renew. Sustain. Ener. Rev., 2012, 16(4), 1883–1891.
- [15] Cervantes-Gaxiola, M.E., Hernandez-Calderon, O.M., Rios-Iribe, E.Y., Rubio-Castro, E., Heat transfer analysis of a non-Newtonian fluid flowing through a Plate Heat Exchanger using CFD, Appl Therm Eng, 2016, 101, 262–272.
- [16] Carvalho E.P., Mota F., Ravagnani M., Optimal design of plate heat exchangers, Applied Thermal Eng., 2014, 63(1), 33–39.
- [17] Datta A., Das A.K., Shyam S., Numerical Analysis of Fluid Flow and Heat Transfer of Flow Between Parallel Plates Having Rectangular Shape Micromixer, J Therm Sci Eng Appl, 2017, 10, DOI: 10.1115/1.4036769
- [18] Entchev E., Ghorab M., Yaici W., 3D CFD analysis of the effect of inlet air flow maldistribution on the fluid flow and heat transfer performances of plate-fin-and tube laminar heat exchangers, Inter. J. Heat Mass Trans., 2014, 74, 490–500.
- [19] Giurgiu O., Plesa A., Socaciu L., 2016, Plate heat exchangers - flow analysis through mini channels, Energy Procedia, 2016, 85, 244–251.
- [20] Jaworski Z., Pianko-Oprych P., 3D CFD fluid flow and thermal analyses of a new design of plate heat exchanger, Polish Journal of Chemical Technology, 2017, 19(1), 17-26.
- [21] Baron, J., Bulewicz, E.M., Chrupek, S., Dzikowska, J., Kandefer, S., Pilawska M., Olek, M., Porzuczek, J., Wrona, J., Żukowski, W., "Sludge for heat," European project presentation, 2007, https://www.kth.se/polopoly_fs/1.650794!/JPS13p61.pdf.
- [22] Baron, J., Bulewicz, E.M., Chrupek, S., Dzikowska, J., Kandefer, S., Pilawska M., Olek, M., Porzuczek, J., Wrona, J., Żukowski, W., European Bio-Energy Projects 1999-2002, 2013, 88–89, http://www.eurosfaire.prd.fr/sustdev/documents/pdf/FP5_european-bio-energy-projects_en_1999-2002.pdf.
- [23] ANSYS Help Viewer: Fluent Theory Guide, ANSYS, Inc., Release 17.2.
- [24] Jaworski Z., Kasilova E., Pianko-Oprych P., Quantification of the radiative and convective heat transfer processes and their effect on mSOFC by CFD modelling, Pol. J. Chem. Technol., 2014, 16(2), 51–55.
- [25] Kalkan O.O., Implementation of k-epsilon turbulence models in a two dimensional parallel navier-stokes solver on hybrid grids MSc Thesis, Middle East Technical University, Turkey, 2014.